

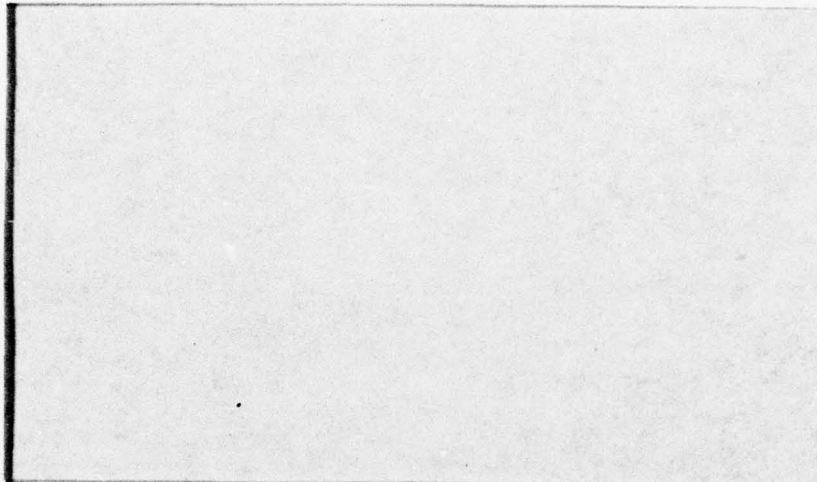
ARO-14254.1-E

LEVEL

12
B.S.

Princeton University

ADAO65131



DDC FILE COPY



[Handwritten signature]

DDC
MAR 1 1978
C

Department of
Mechanical and
Aerospace Engineering

This document has been approved
for public release and sale; its
distribution is unlimited.

79 02 26 007

Ref: MAE Rept. #1421 ✓

12

A065131

SUPERSONIC, HIGH REYNOLDS NUMBER FLOW OVER
A TANGENT OGIVE CYLINDER AT SMALL ANGLES OF ATTACK:
AN EXPERIMENTAL STUDY AND COMPARISON WITH THEORY

by

D. S. Dolling
S. M. Bogdonoff

INTERIM TECHNICAL REPORT
U. S. ARMY RESEARCH GRANT DAAG29-77-G-0234

DDC
MAR 1 1979
C

DDC FILE COPY

This document has been approved
for public release and sale; its
distribution is unlimited.

January 1979

79 02 26 007

ABSTRACT

↓
An experimental investigation ^{was} ~~has been~~ made of the flow over a tangent ogive cylinder model ^{small} at angle of attack. The model was approximately 10 calibers (50cm, 20ⁱⁿ) long with a 3 caliber nose. Surface pressure distributions have been measured in both the circumferential and axial directions and boundary layer pitot surveys made at four stations along the wind and lee sides of the cylinder. Over the entire angle of attack range tested, ⁰ ~~0~~ through ^{5 deg} ~~5~~, no boundary layer separation was observed.

^{10 to the 7th power / m ± (1.6 million/in.)}
All the measurements were made at a nominal freestream Mach number of 3, a unit Reynolds number of $6.2 \times 10^7 \text{ m}^{-1}$ ($1.6 \times 10^6 \text{ in}^{-1}$) and with near adiabatic wall conditions. At these high Reynolds numbers, natural boundary layer transition occurred, and in all cases was observed close to the nose tip.

The measurements ^{were} ~~have been~~ compared with predictions from a boundary layer based computer code developed by Sturek, et al, at the U. S. Army Ballistic Research Laboratories. Pressure distributions agree well with the predictions. The experimental and computed velocity profiles have some common trends but there exist significant discrepancies between them. In a general sense, the computed and measured profiles have fundamentally different shapes and their downstream development is not accurately modelled, particularly on the windside.

TABLE OF CONTENTS

	<u>Page</u>
ABSTRACT	i
TABLE OF CONTENTS	ii
LIST OF FIGURES	iii
NOMENCLATURE	iv
1. INTRODUCTION	1
2. EXPERIMENTAL PROGRAM	3
2.1 Wind Tunnel Facility	3
2.2 Model Description	3
2.3 Surface Pressure Distributions	4
2.4 Boundary Layer Surveys	4
2.5 Additional Measurements	5
2.6 Estimated Measurement Uncertainties	5
3. DISCUSSION OF THE DATA AND COMPARISON WITH THEORY	6
3.1 Surface Pressure Distribution	6
3.2 Boundary Layer Velocity Profiles	7
4. CONCLUDING REMARKS	9
5. REFERENCES	10
FIGURES	

LIST OF FIGURES

<u>Figure No.</u>	<u>Title</u>
1	Model Schematic and Coordinate System.
2	Pressure Distributions at Zero Angle of Attack.
3	Pressure Distributions at 4° Angle of Attack.
4	Boundary Layer Velocity Profiles ($\alpha = 0^\circ$).
5	Boundary Layer Velocity Profiles ($\alpha = 2^\circ$, $\phi = 0^\circ$).
6	Boundary Layer Velocity Profiles ($\alpha = 2^\circ$, $\phi = 180^\circ$).
7	Boundary Layer Velocity Profiles ($\alpha = 4^\circ$, $\phi = 0^\circ$).
8	Boundary Layer Velocity Profiles ($\alpha = 4^\circ$, $\phi = 180^\circ$).
9	Boundary Layer Velocity Profiles ($\alpha = 5.1^\circ$, $\phi = 0^\circ$).
10	Boundary Layer Velocity Profiles ($\alpha = 5.1^\circ$, $\phi = 180^\circ$).
11	Comparison of Experimental and Theoretical Streamwise Boundary Layer Development ($\alpha = 4^\circ$, $\phi = 0^\circ$).
12	Comparison of Experimental and Theoretical Streamwise Boundary Layer Development ($\alpha = 4^\circ$, $\phi = 180^\circ$).
13	Streamwise Boundary Layer Displacement Thickness Growth.

NOMENCLATURE

D	diameter of cylindrical portion of the model
M	freestream Mach number ahead of the model
P _{WALL}	local measured wall pressure
P _{STATIC}	freestream static pressure ahead of the model
RE	freestream unit Reynolds number ahead of the model
U	local velocity in the boundary layer
U _E	velocity at the boundary layer edge
X	coordinate measured along the model axis with origin at the ogive tip
Y	distance measured from the model surface
α	model angle of attack
δ^*	boundary layer displacement thickness
ϕ (PHI)	coordinate measured in circumferential direction (degrees)

1. INTRODUCTION

One of the many objectives of computational fluid dynamics has been the calculation of the flowfield around an axisymmetric body at angle of attack in a supersonic stream. The case of a spinning body is of particular practical interest. In such cases the interaction of the surface spin with the crossflow velocity modifies the three-dimensional boundary layer displacement surface giving rise to an asymmetric pressure distribution. The resultant side force, the Magnus force, is small (typically 1/10 to 1/100 of the normal force), but is important because its moment may be large enough to render the body dynamically unstable. Satisfactory prediction of the Magnus force clearly hinges on accurate modelling of the turbulent boundary layer development on the body.

To guide such computational procedures there is a need for detailed boundary layer profile data, both on spinning and non-spinning bodies, particularly at the high Reynolds numbers representative of flight. The present experimental study, carried out using a non-spinning model, is similar to some earlier investigations (Refs. 1-5), but is at much higher Reynolds numbers. Surface pressure distributions and boundary layer velocity profiles have been measured on a tangent ogive cylinder model at angle of attack in a high Reynolds number supersonic ($M = 3$) flow. As far as is known, no other similar data are available at such high Reynolds numbers.

In this report, comparisons are made between the experimental data and predictions from a computational scheme developed by Sturek, et al, at the U. S. Army Ballistic Research Laboratories. Input for the code consisted

of the exact body geometry and freestream conditions used in the test program. Emphasis here is on the comparisons and no discussion of the codes is given. The code structure, the governing equations, the turbulent shear stress model necessary for closure, etc., is discussed in detail by Sturek, et al, in Ref. 6.

2. EXPERIMENTAL PROGRAM

2.1 Wind Tunnel Facility

The experimental study was carried out in the Princeton University high Reynolds number supersonic blowdown tunnel. This tunnel has a test section 20 cm x 20 cm (8" x 8"), a nominal freestream Mach number of 3 and may be operated at stagnation pressures in the range $4 \times 10^5 \text{ Nm}^{-2}$ to $3.4 \times 10^6 \text{ Nm}^{-2}$ (60-500 psia).

In this study, all tests were carried out at a stagnation pressure of $6.8 \times 10^5 \text{ Nm}^{-2}$ (100 psia) giving a freestream unit Reynolds number of $6.2 \times 10^7 \text{ m}^{-1}$ ($1.6 \times 10^6 \text{ in}^{-1}$). The models were at near adiabatic wall temperature for all tests.

2.2 Model Description

The model used was a tangent-ogive cylinder of diameter 5.08 cm (2") and overall length about 50 cm (20"). The ogive nose section was approximately 3 calibers in length. A schematic of the model and the coordinate system to be used for data presentation is shown in Fig. 1.

It was instrumented with 140 pressure tapings distributed in 7 rows along the cylinder body from $\phi = 0^\circ$ to $\phi = 180^\circ$ in increments in ϕ of 30° . Each row consisted of 20 tapings spaced at 1/4 caliber intervals with the first and last ports being located at X/D's of 2.925 and 7.675 respectively. Six additional circumferential pressure tapings were used for aligning the model at zero angle of attack to the incoming freestream direction. Three flush mounted chromel-alumel thermocouples were installed for monitoring the model wall temperature history during a run.

The model was secured in the tunnel using an axial sting located aft of the cylinder body. A ball-joint type adapter at the sting/model interface permitted a model angle of attack in the range $-5.1^\circ \leq \alpha \leq +5.1^\circ$.

2.3 Surface Pressure Distributions

Pressure distributions were measured along all 7 rows of tappings for model angles of attack 0° , 2° , 4° and 5.1° (the maximum attainable). The zero angle of attack setting was obtained iteratively by equalizing the pressures measured at ports located at $\phi = 0^\circ$, 90° , 180° and 270° . Other angles of attack were obtained geometrically by displacing the ogive tip a pre-calculated distance from the tunnel floor. The ball joint adapter was designed so that this motion was constrained in the vertical plane. As a check on flow uniformity and measurement repeatability, complete sets of pressure distributions were made both with the model on the test section axis and 2.54 cm (1") off it. Excellent repeatability was obtained.

2.4 Boundary Layer Surveys

Boundary layer pitot pressure surveys were made at 4 stations ($X/D = 3.175$, 3.925 , 4.925 and 6.925) along the wind and leeside rays of the model. The surveys were made using a flattened hypodermic needle probe with a height of .18mm (.007"). Data were taken at the same 4 angles of attack as in the pressure measurements study.

Tests made to assess model wall/pitot probe interference indicated that it occurred at distances less than about $1\frac{1}{2}$ probe heights above the wall. In reducing the pitot pressure surveys to velocity profiles the local measured value of wall static pressure was used and assumed to be constant through the boundary layer.

2.5 Additional Measurements

The flow total pressure, total temperature, and model wall temperature history were recorded for all tests. For consistency all tests were started with approximately the same wall temperature, which was close to the adiabatic value.

Shadow and schlieren photographs were taken at all angles of attack. The approximate locations of boundary layer transition on the wind and leeside rays could thus be estimated. At these high Reynolds numbers, transition was always natural and occurred close to the ogive tip.

2.6 Estimated Measurement Uncertainties

Based on the small difference between the four measured circumferential pressures the model zero angle of attack setting is estimated as being accurate to order $\pm 0.1^\circ$. Errors in the geometric angle setting technique, coupled with the zero setting error indicates an overall uncertainty of about 0.15° at angle of attack. During the tunnel start up and run no offset from the static angle of attack setting was detectable.

Static and pitot pressures were repeatable from test to test and have an estimated uncertainty of order 1-2%. The overall accuracy of the absolute probe displacement from the model surface is about .08mm (.003"). This represents about .056 for the thinnest boundary layer measured and less than .016 for the thickest.

3. DISCUSSION OF THE DATA AND COMPARISON WITH THEORY

The major set of comparisons presented here are between the measured and predicted boundary layer velocity profiles. Overall surface properties, such as pressure distributions can be reasonably well calculated using inviscid theory, and are therefore not very satisfactory criteria for judging the predictive abilities of a boundary layer computational scheme. For the angle of attack range covered in the test program no flow separation was observed.

3.1 Surface Pressure Distributions

Figure 2 shows a comparison of the measured and predicted pressure distribution at zero angle of attack. The solid lines correspond to the predictions. The lower line is the pressure distribution due to the "body alone" whereas the upper line is due to the geometry corresponding to the "body plus the boundary layer displacement surface". Experimentally, the results exhibit some random scatter and are consistently a few per cent higher than the predictions. Some of the scatter is caused by the impingement of weak waves emanating from small disturbances such as tunnel section joints. At such high Reynolds numbers, the boundary layer is very thin such that their impingement results in small irregularities in the pressure distribution.

Pressure distributions for all seven values of ϕ , for the model at 4° angle of attack are shown in Fig. 3. Again, predictions for the "body alone" and "body with displacement surface" are shown, with the latter being the upper solid line. Note that the pressure axis scale is correct for the $\phi = 0^\circ$ data set. The other data are staggered upwards, with the $\phi = 30^\circ$ data shifted 0.25 pressure units, the $\phi = 60^\circ$ by 0.50 units, etc. Agreement is good in both the streamwise and circumferential directions.

From these and other comparisons at 2° and 5° angle of attack it is apparent that the overall trends of the pressure distribution with X/D , ϕ and α are satisfactorily predicted by the code. On the cylindrical part of the model, the "body alone" solution differs little from the "body plus displacement surface" one. The former, which is simply the basic inviscid solution appears capable of predicting the pressure distribution, at least over the angle of attack range tested.

3.2 Boundary Layer Velocity Profiles

Boundary layer velocity profiles on the wind and leeward rays at model angles of attack of 0° , 2° , 4° and 5.1° are shown in Figs. 4 through 10. Each figure shows comparisons of the experimental profiles with the theoretical ones at four body stations (#'s 2, 5, 9 and 15). The solid line is the predicted profile.

At angle of attack, on the leeside, the theoretical velocities tend to be higher than the measured ones near the wall, and less than them near the boundary layer edge. The predicted boundary layer thicknesses are also consistently higher than the measured ones. On the windside, the overall trend is for the theoretical velocities to be less than those measured throughout the profile. Again, the theoretical boundary layer thicknesses are higher.

The leeside trend noted above was also observed by Kayser and Sturek (Ref. 5). In their comparisons with experiment, the opposite trend occurred on the windside, which is not the case seen here. Their experimental program, also at a freestream Mach number of 3, used a 6 caliber secant-ogive cylinder model, with a 3 caliber nose. The freestream unit Reynolds number was about 35% of that in the present program, and the model was equipped with a boundary

layer trip located 0.7 calibers from the nose tip. Overall, comparisons of their experimental data with predictions are better, particularly on the windside of the model. In general, the higher Reynolds number data of the present study are not well predicted, particularly at angle of attack. At zero angle of attack (Fig. 4), the comparisons are good over most of the profile, except for station 2 ($X/D = 3.175$) which is immediately downstream of the ogive/cylinder shoulder.

Composite plots, illustrating the effects of changes in α or X/D on the profiles, reveal some significant differences between the predictions and the measurements. An example is shown in Fig. 11, where the four theoretical and measured windside profiles are shown for a model angle of attack of 4° . The two sets of profiles differ not only in their development with increasing X/D but also in their basic shape. On the leeward side (Fig. 12), the computations model the overall development of the profile with increasing distance downstream, but again the basic shape of the profile is different. The theoretical profiles, both on the windside and leeward side, have a noticeably curved shape, whereas the experimental profiles are much more linear with a more abrupt change in curvature near the boundary layer edge.

The corresponding growth of the boundary layer displacement thickness δ^* is shown in Fig. 13. As would be expected from the theoretical windside profiles of Fig. 11, δ^* is almost constant along the body. From station 2 to station 15 the theoretical δ^* increases by about 14% whereas the experimental data show a growth of over 50%. On the leeward side the differences are even more noticeable. The experimental values are consistently higher (by about 20% at station 2 and 40% at station 15) and have a greater growth rate. The zero angle of attack data plotted on the same figure also have a similar trend.

4. CONCLUDING REMARKS

Comparisons have been made between experimental and theoretical pressure distributions and boundary layer velocity profiles on a tangent ogive cylinder model. Data are compared over the angle of attack range 0° through 5° in a high Reynolds number supersonic ($M = 3$) flow. No boundary layer separation was observed.

The computed pressure distributions agree well with the measured ones. In these unseparated cases the purely inviscid solution seems adequate. The experimental and computed velocity profiles have some common trends but there exist significant discrepancies between them. In a general sense, the computed and measured profiles have fundamentally different shapes and their downstream development is not accurately modelled, particularly on the wind-side.

5. REFERENCES

1. Sturek, W. B., "Preliminary Surveys of the Three-Dimensional Boundary Layer on a Yawed Spinning Body of Revolution", U.S.A. Ballistic Research Laboratories, Memorandum Report No. 2501, July 1975.
2. Sturek, W. B. and Reba, J. J., "Measurements of Wall Static Pressure on a Yawed Tangent Ogive Cylinder", U.S.A. Ballistic Research Laboratories, Memorandum Report No. 2699, November 1976.
3. Sturek, W. B. and Danberg, J. E., "Experimental Measurements of the Turbulent Boundary Layer on a Yawed, Spinning, Slender Body", U.S.A. Ballistic Research Laboratories, Report No. 1954, January 1977.
4. Kayser, L. D., Yanta, W. J. and Sturek, W. B., "Measurements in the Turbulent Boundary Layer of a Yawed, Spinning Body of Revolution at Mach 3.0 with a Laser Velocimeter and Impact Probe", U.S.A. Ballistic Research Laboratories, Technical Report ARBRL-TR-02074, May 1978.
5. Kayser, L. D. and Sturek, W. B., "Experimental Measurements in the Turbulent Boundary Layer of a Yawed, Spinning Ogive-Cylinder Body of Revolution at Mach 3.0. Part I: Description of the Experiment and Data Analysis", U.S.A. Ballistic Research Laboratories, Memorandum Report ARBRL-MR-02808, January 1978.
6. Sturek, W. B., et al., "Computations of Magnus Effects for a Yawed Spinning Body of Revolution", AIAA J., Vol. 16, No. 7, July 1978, pp. 687-692.

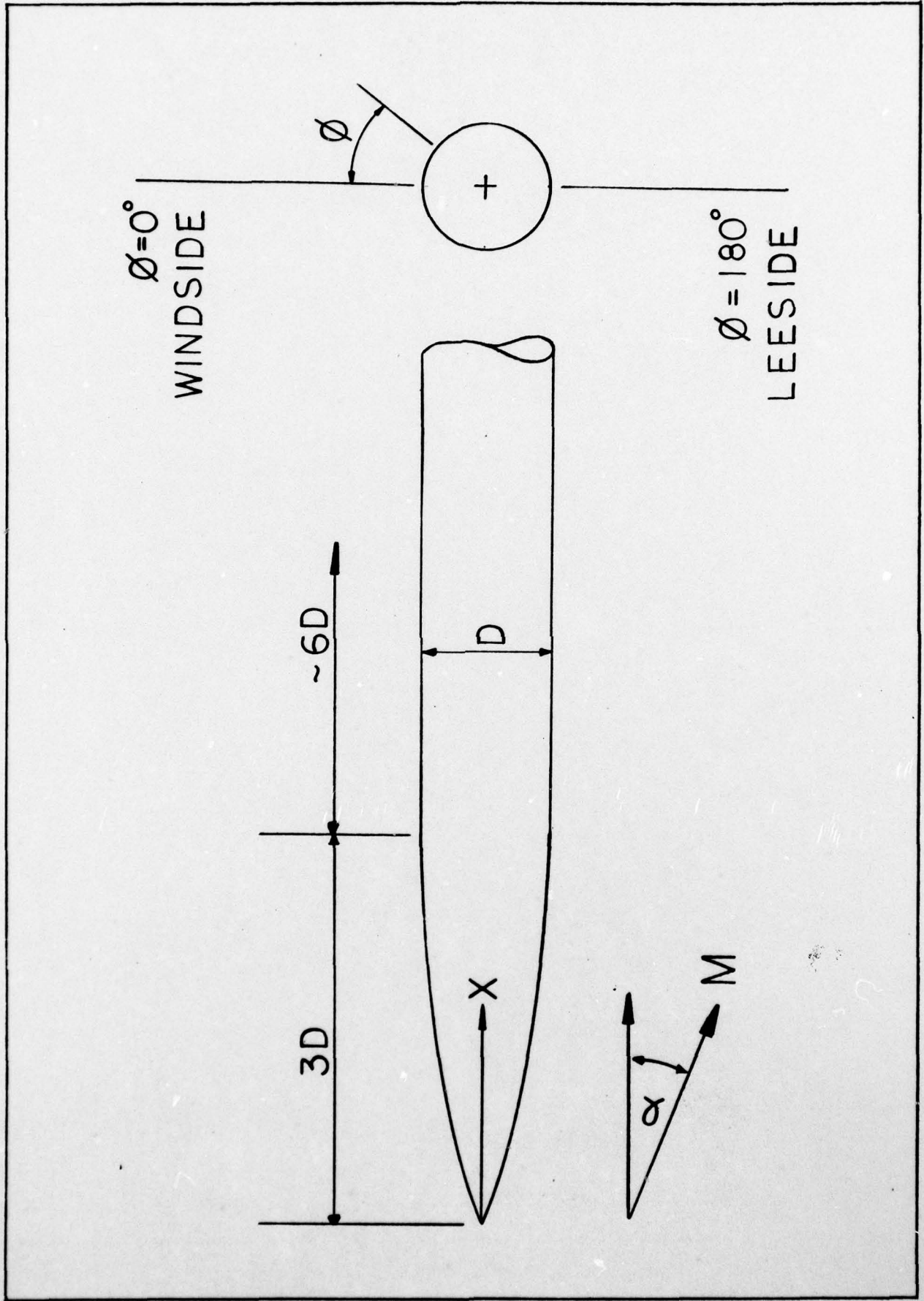


FIG. 1. MODEL SCHEMATIC AND COORDINATE SYSTEM.

TGT. OGIVE CYLINDER STUDY

M=2.95 RE=6.3×10⁶ M-1
INCIDENCE=0

PHI

- 0.0
- 30.0
- △ 60.0
- + 90.0
- X 120.0
- ◇ 150.0
- ↑ 180.0

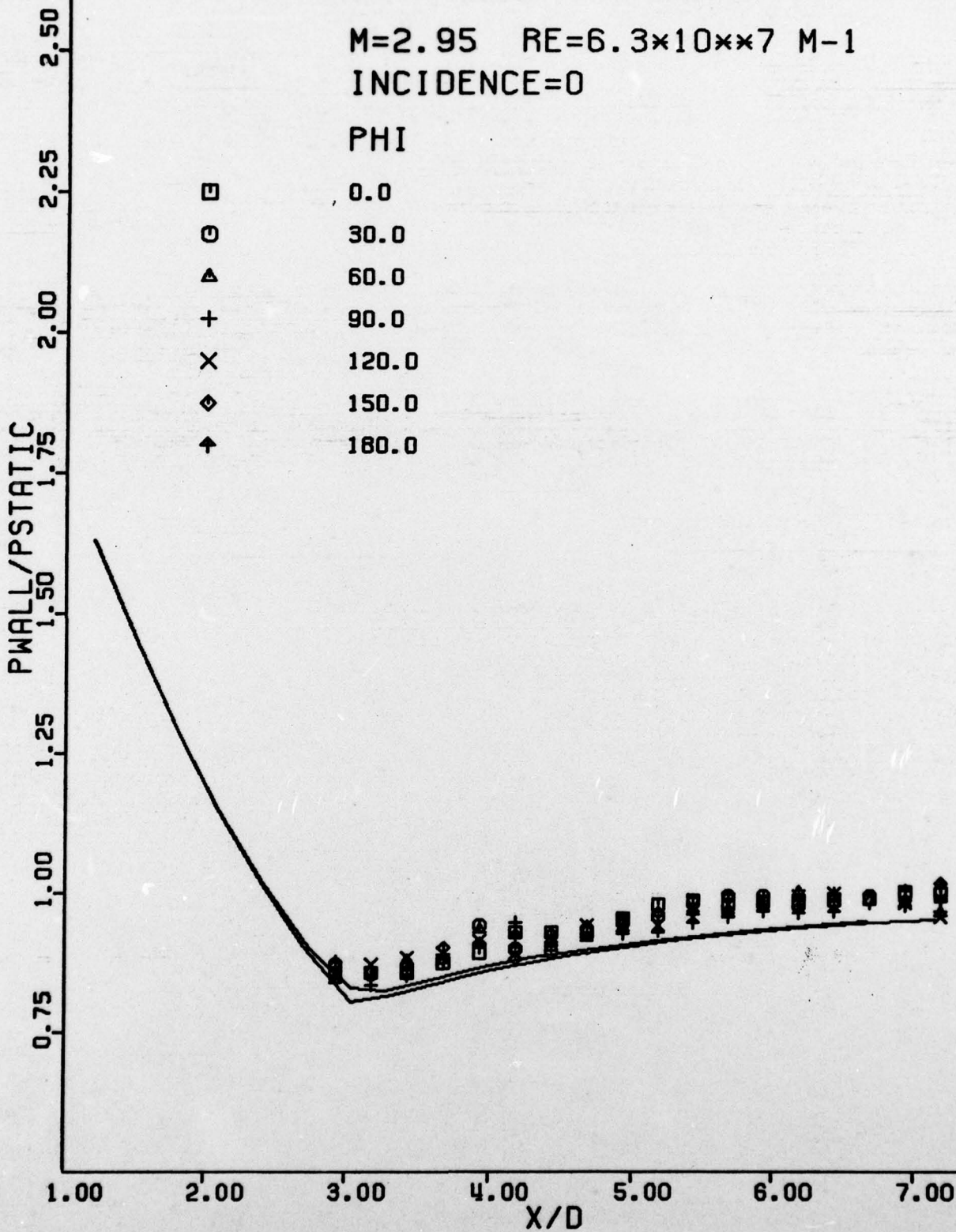


FIG. 2. PRESSURE DISTRIBUTIONS AT ZERO ANGLE OF ATTACK.

TGT. OGIVE CYLINDER STUDY
M=2.95 RE=6.3×10××7 M-1
INCIDENCE=4 DEGREES

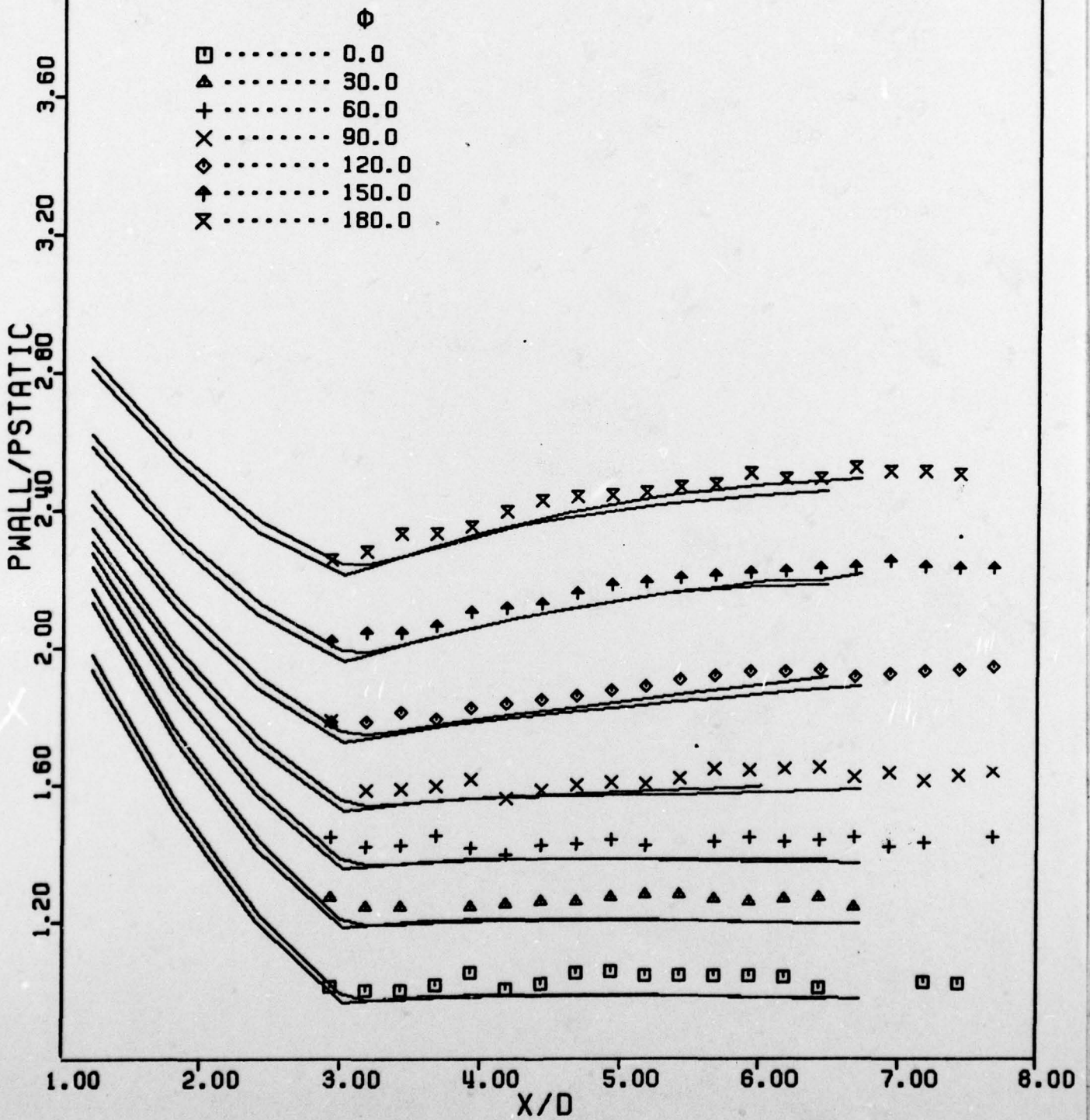


FIG. 3. PRESSURE DISTRIBUTIONS AT 4° ANGLE OF ATTACK.

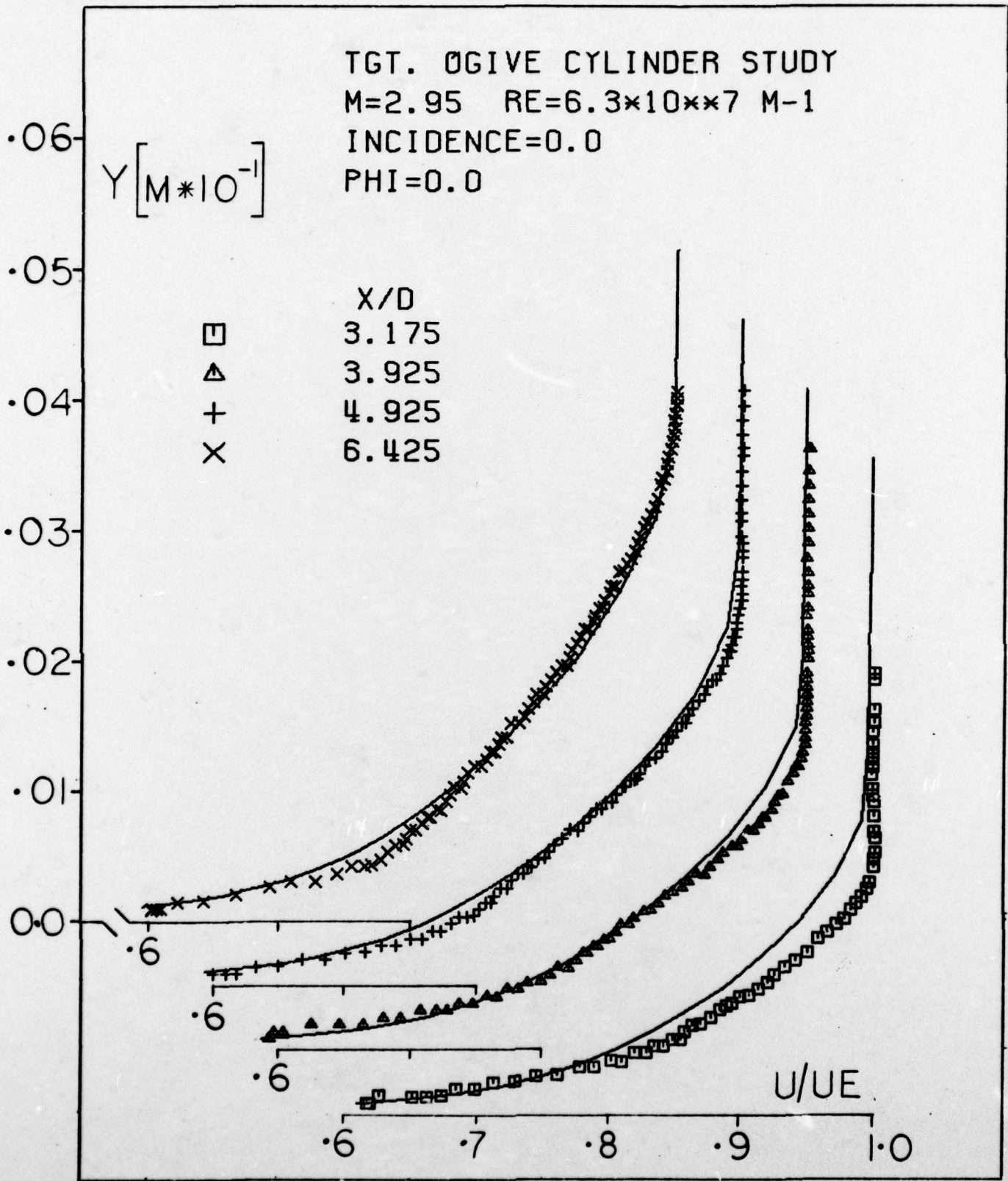


FIG. 4. BOUNDARY LAYER VELOCITY PROFILES ($\alpha = 0^\circ$).

TGT. OGIVE CYLINDER STUDY
 M=2.95 RE=6.3×10⁶ M-1
 INCIDENCE=2.0
 PHI=0.0

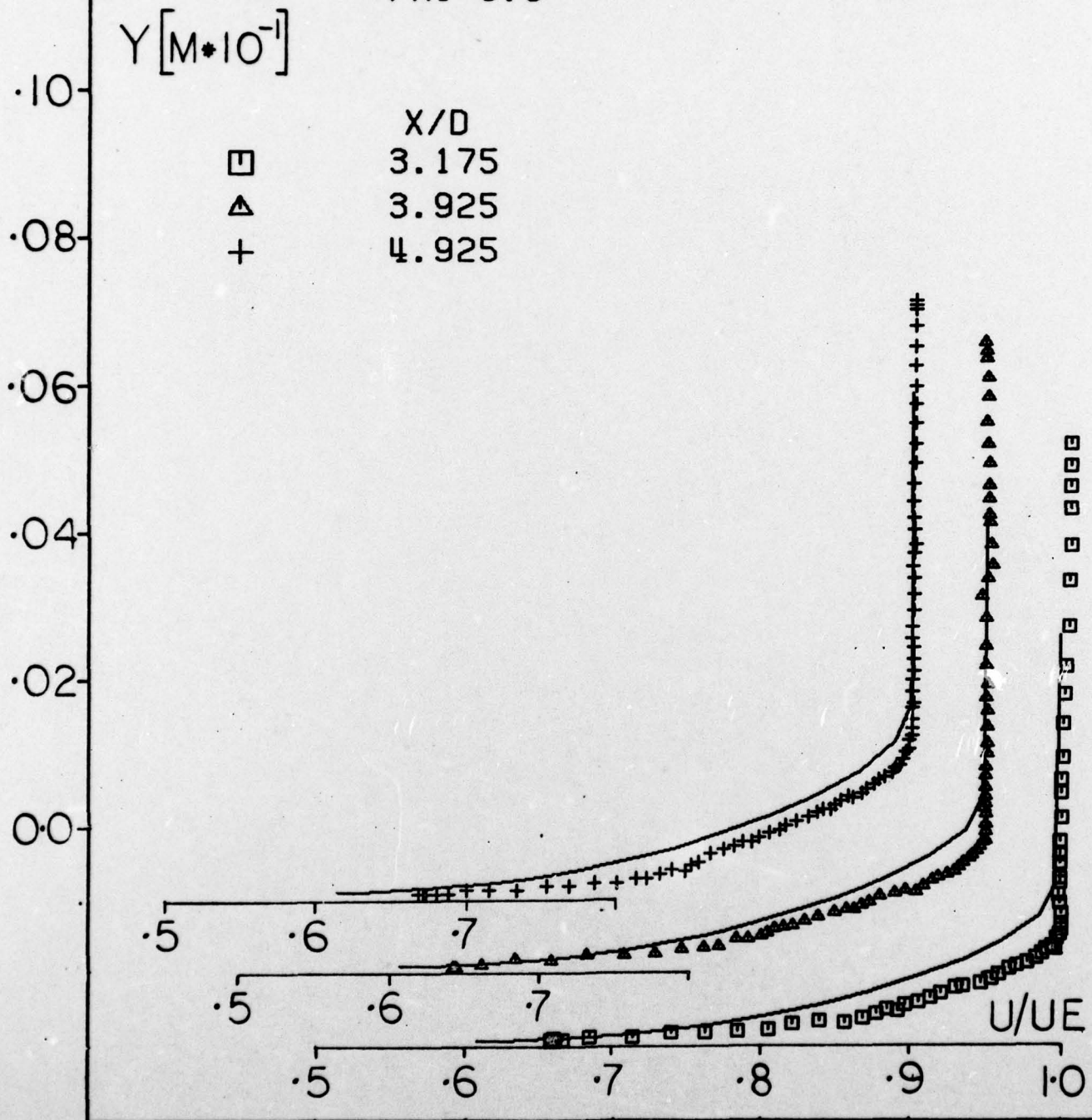


FIG. 5. BOUNDARY LAYER VELOCITY PROFILES ($\alpha = 2^\circ$, $\phi = 0^\circ$).

TGT. OGIVE CYLINDER STUDY

M=2.95 RE=6.3×10⁶ M-1

INCIDENCE=2.0

PHI=180.0

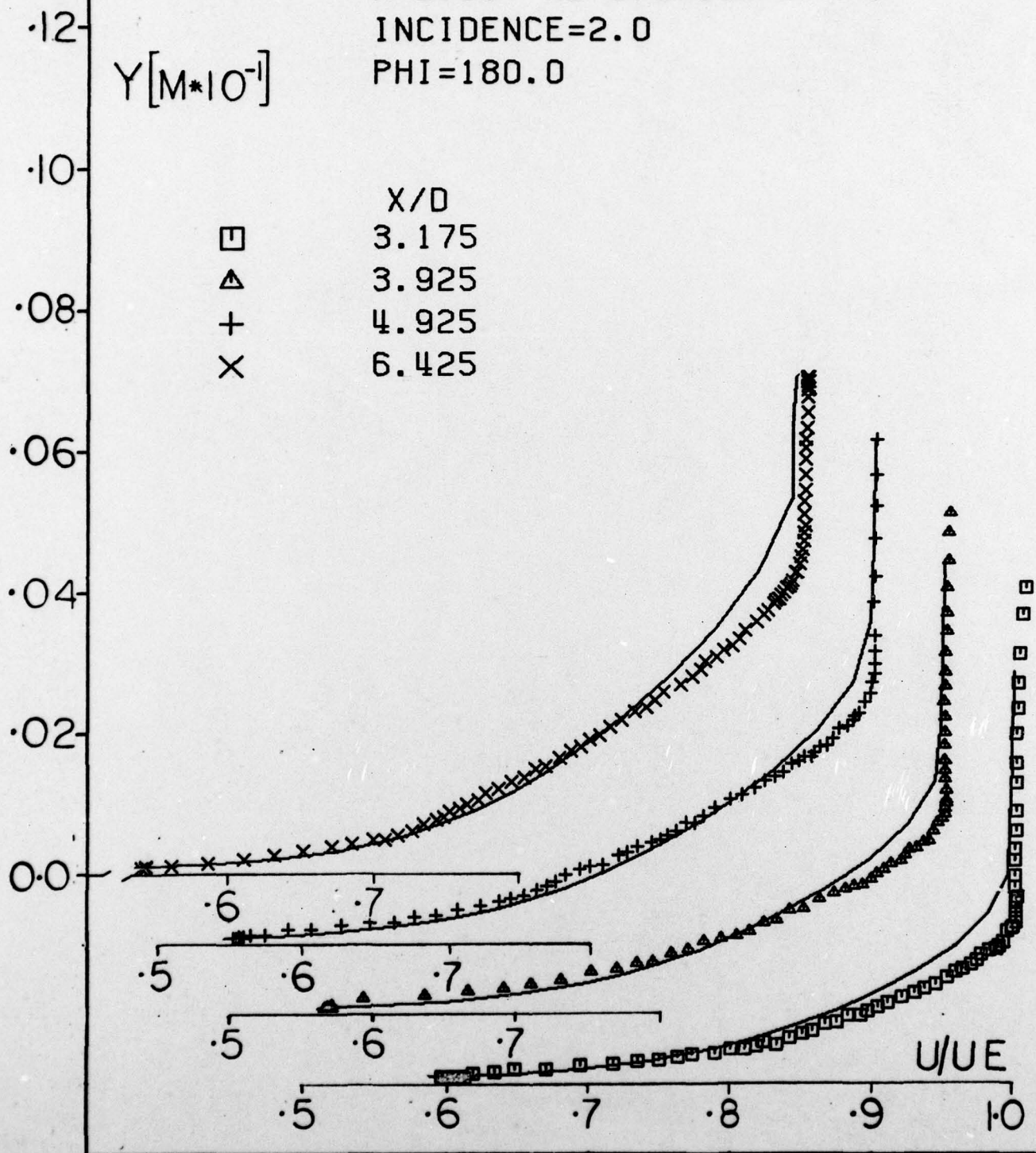


FIG. 6. BOUNDARY LAYER VELOCITY PROFILES ($\alpha = 2^\circ$, $\phi = 180^\circ$).

TGT. OGIVE CYLINDER STUDY
M=2.95 RE=6.3×10⁶ M-1
INCIDENCE=4.0
PHI=0.0

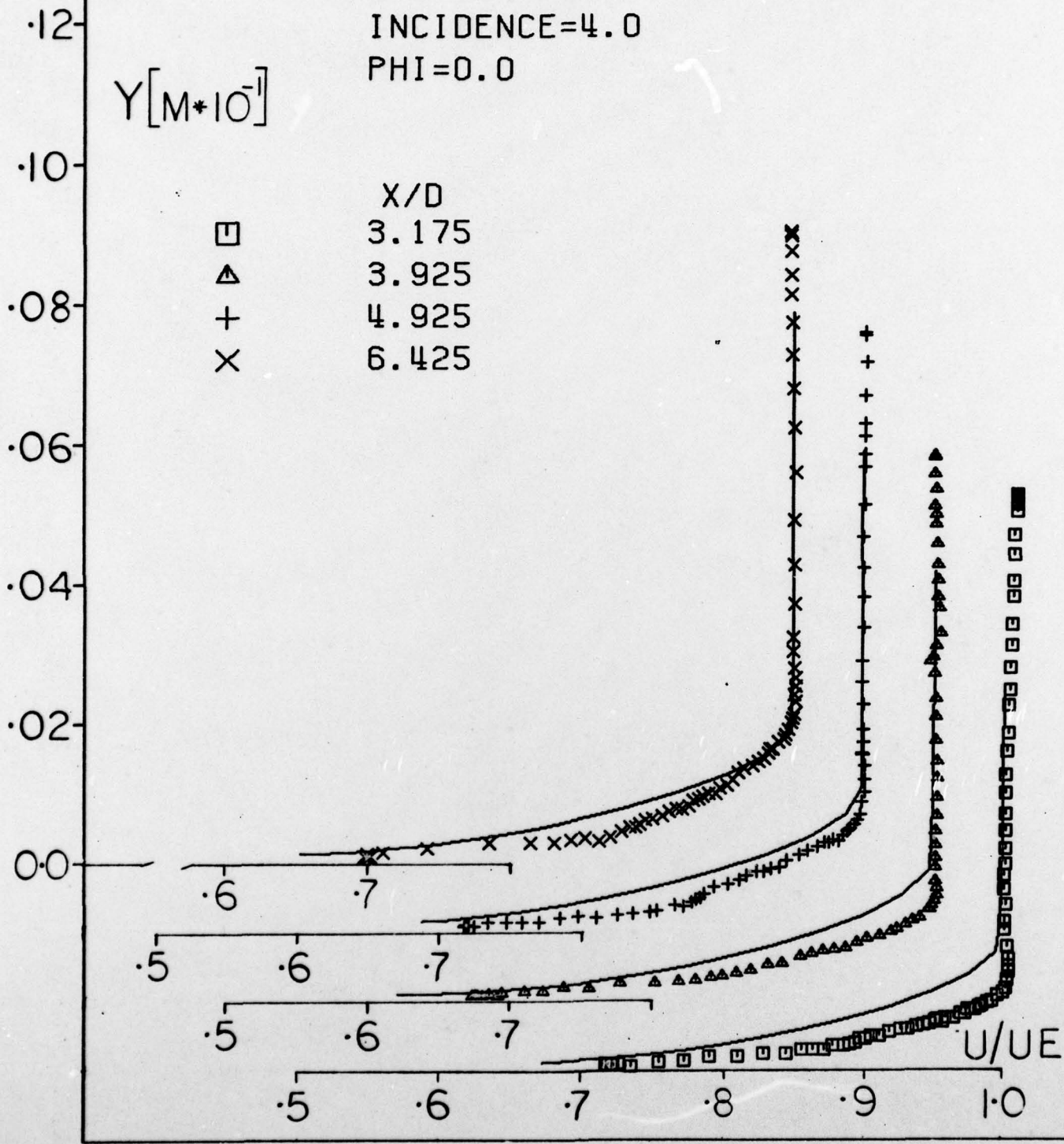


FIG. 7. BOUNDARY LAYER VELOCITY PROFILES ($\alpha = 4^\circ$, $\phi = 0^\circ$).

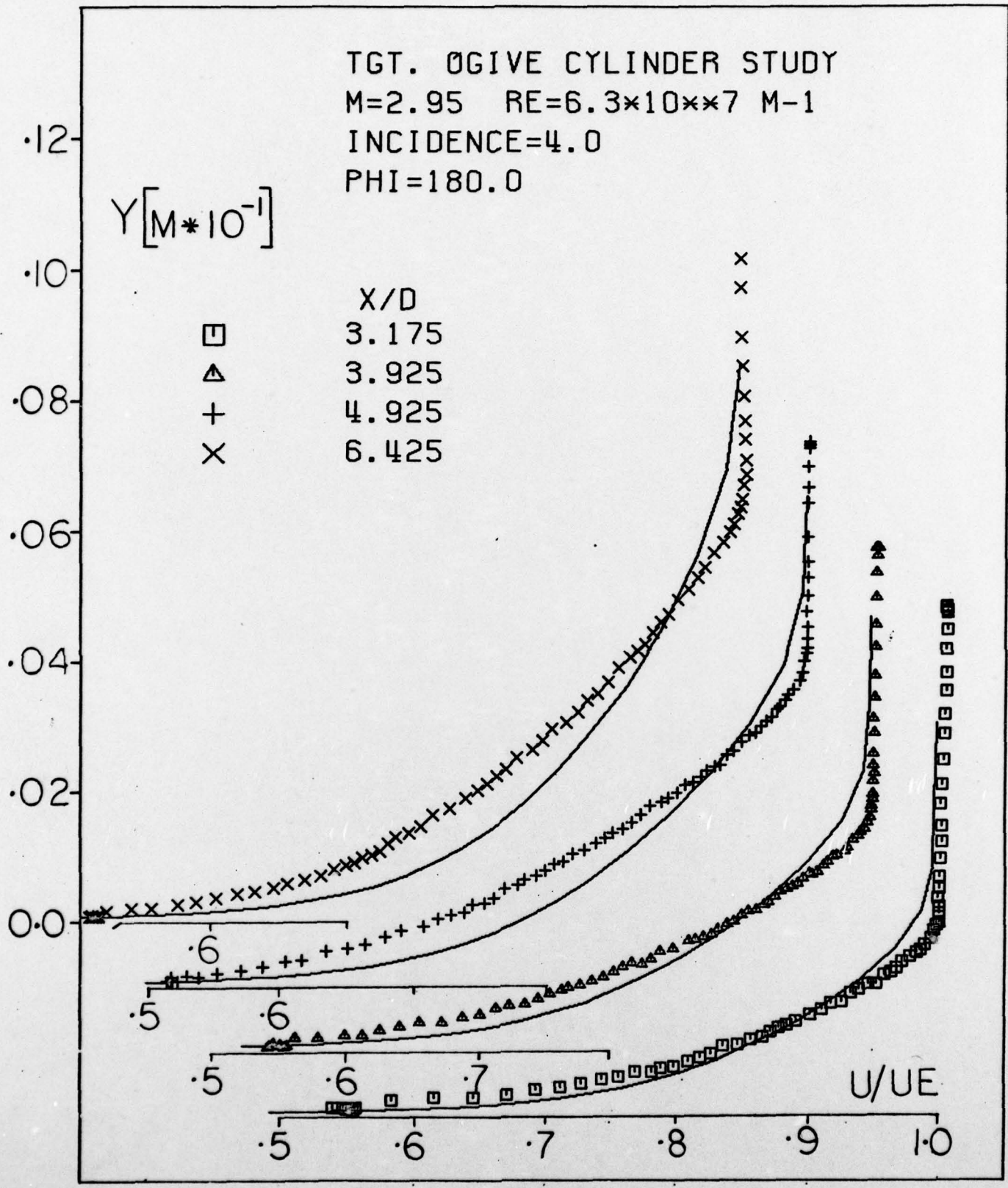


FIG. 8. BOUNDARY LAYER VELOCITY PROFILES ($\alpha = 4^\circ$, $\phi = 180^\circ$).

TGT. OGIVE CYLINDER STUDY
 $M=2.95$ $RE=6.3 \times 10^6$
 INCIDENCE=5.1
 PHI=0.0

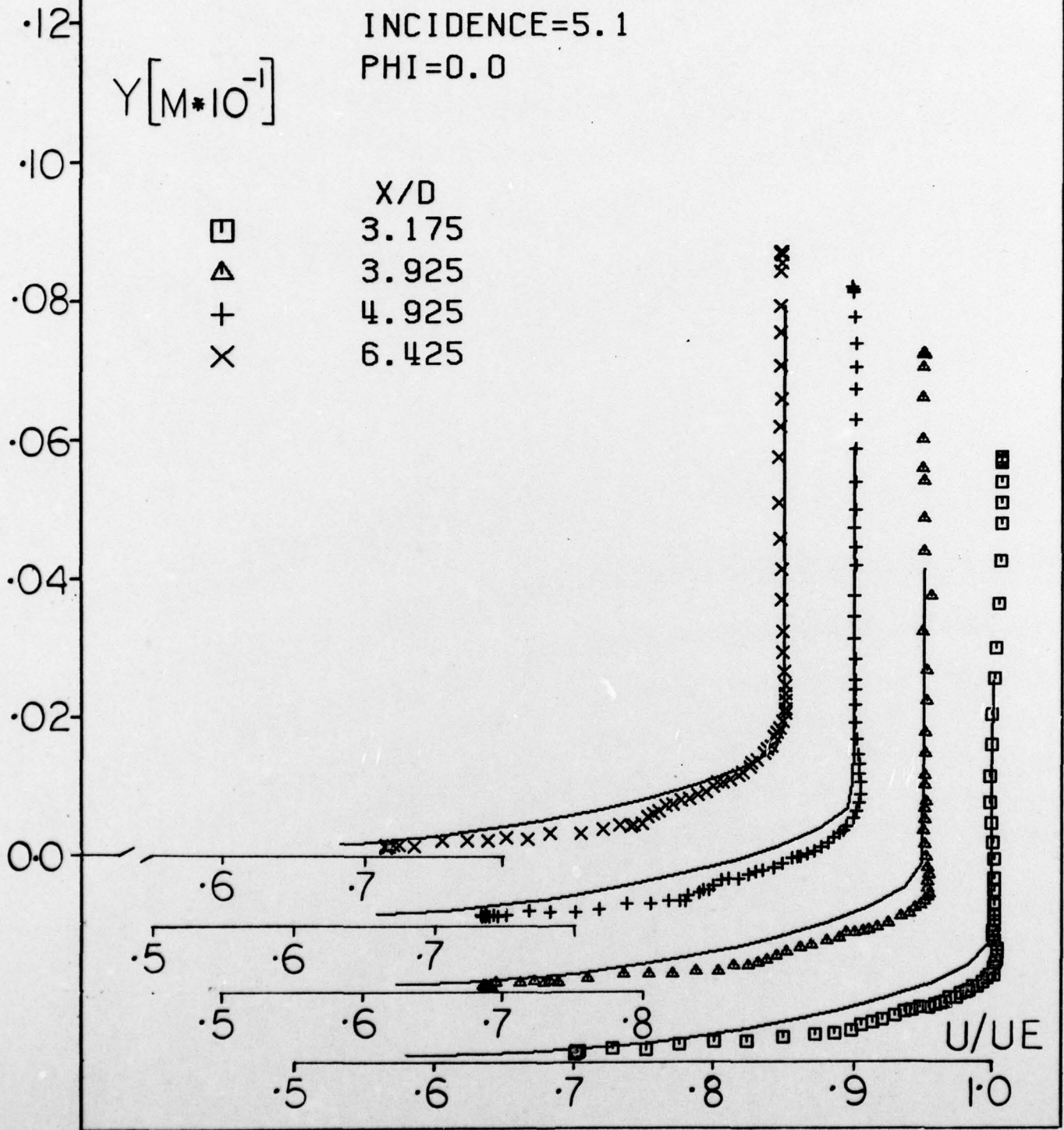


FIG. 9. BOUNDARY LAYER VELOCITY PROFILES ($\alpha = 5.1^\circ$, $\phi = 0^\circ$).

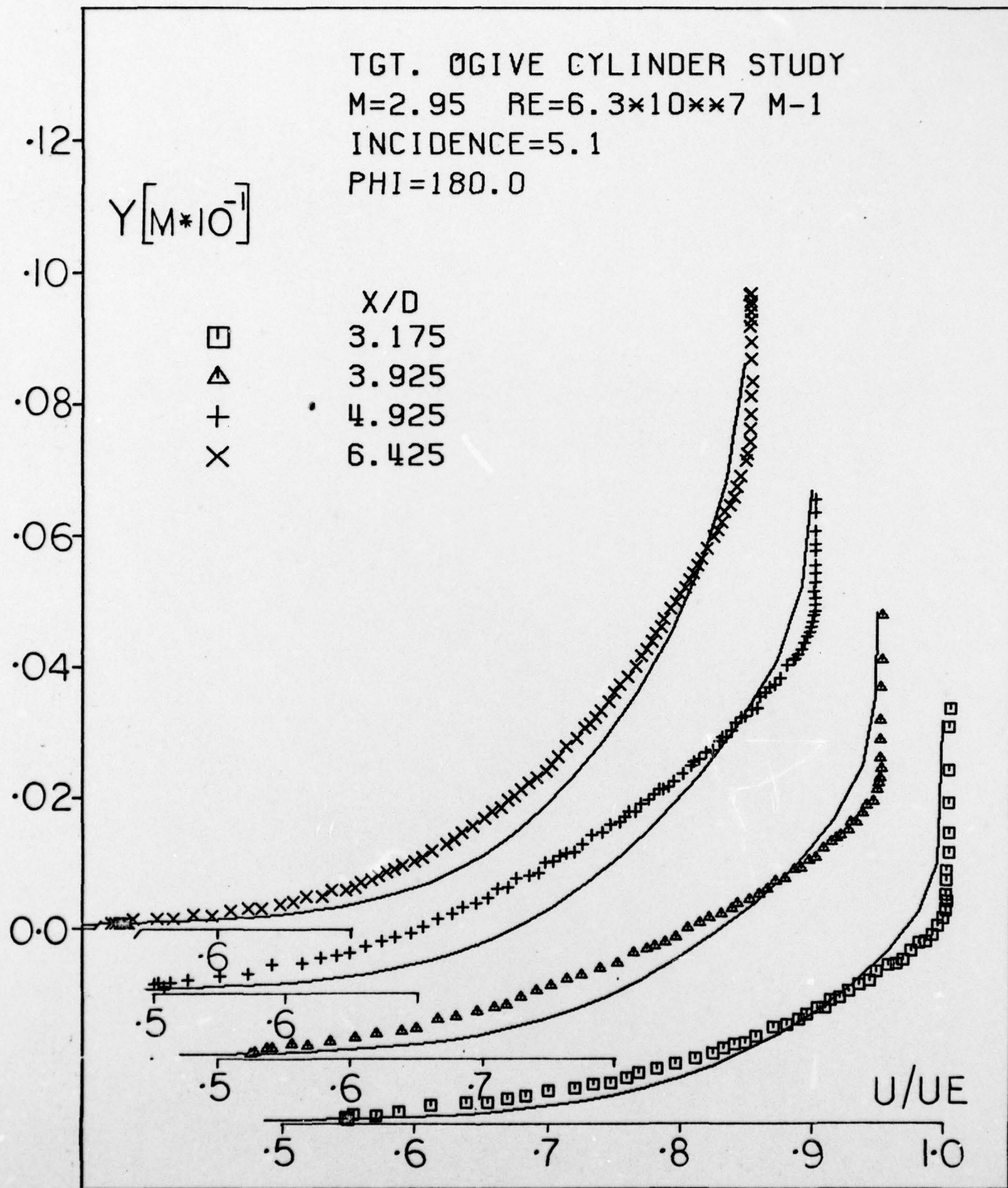


FIG. 10. BOUNDARY LAYER VELOCITY PROFILES ($\alpha = 5.1^\circ$, $\phi = 180^\circ$).

TGT. OGIVE CYLINDER STUDY

M=2.95 RE=6.3×10⁴ M-1

INCIDENCE=4.0

PHI=0.0

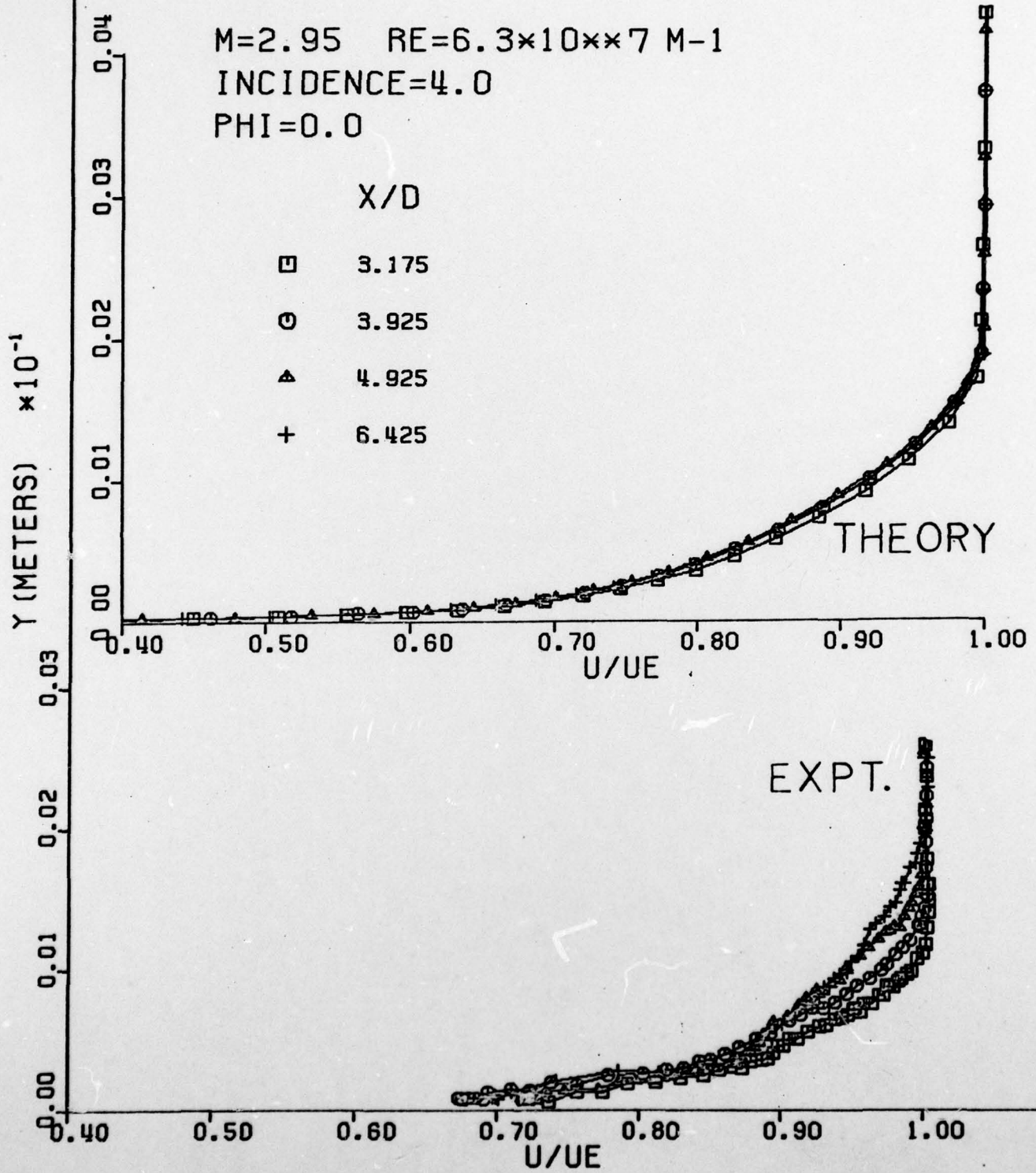


FIG. 11. COMPARISON OF EXPERIMENTAL AND THEORETICAL STREAMWISE BOUNDARY LAYER DEVELOPMENT ($\alpha = 4^\circ$, $\phi = 0^\circ$).

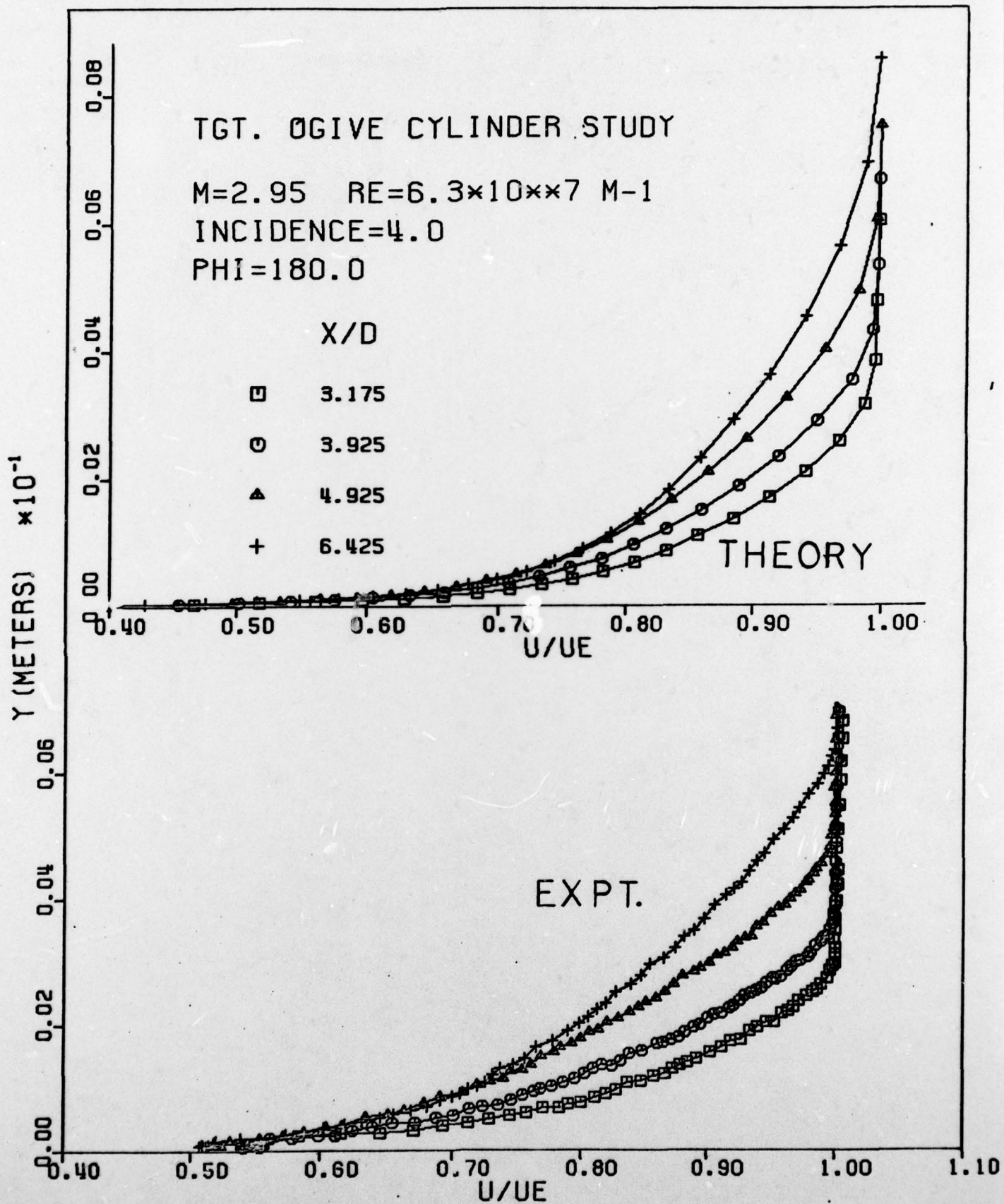


FIG. 12. COMPARISON OF EXPERIMENTAL AND THEORETICAL STREAMWISE BOUNDARY LAYER DEVELOPMENT ($\alpha = 4^\circ$, $\phi = 180^\circ$).

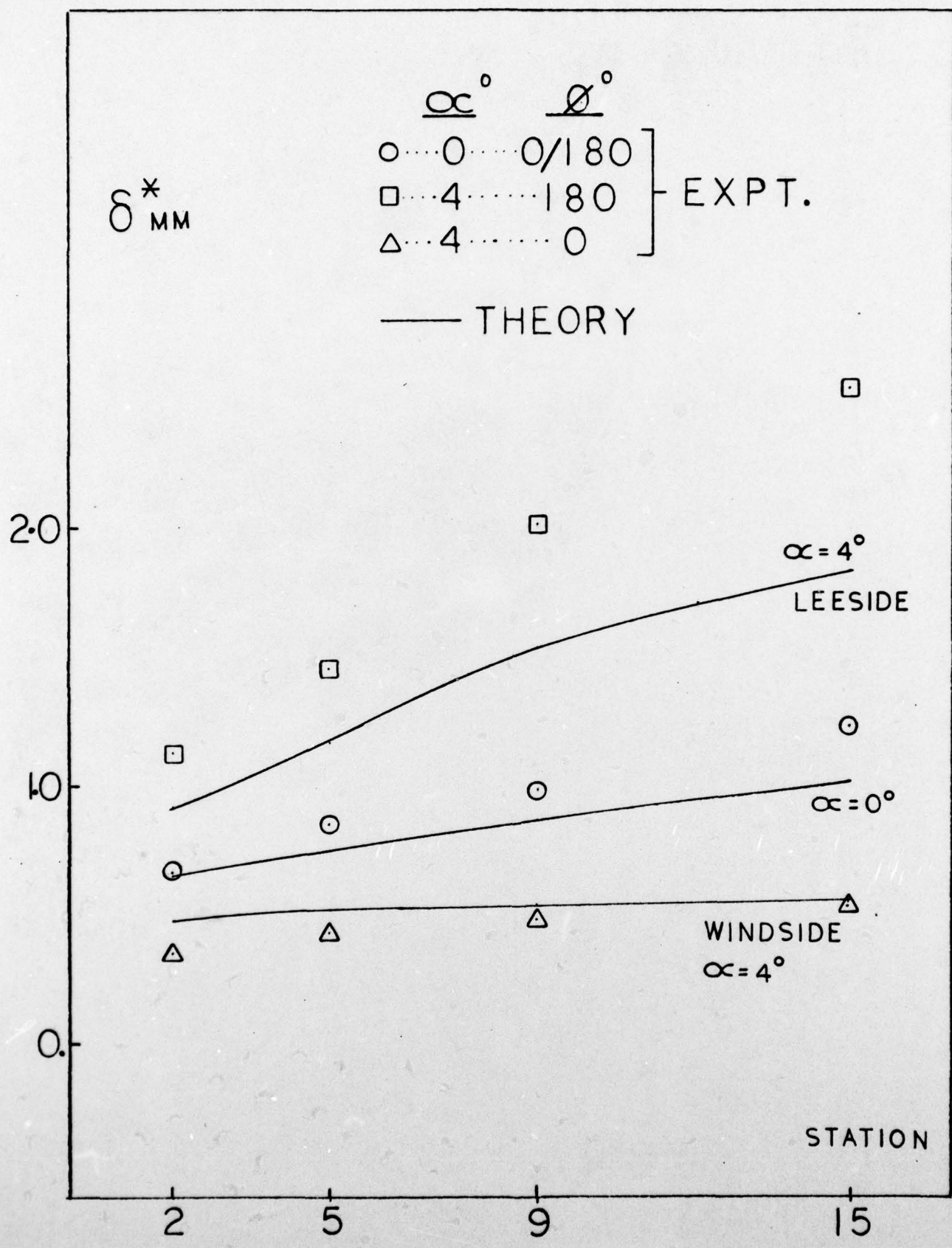


FIG. 13. STREAMWISE BOUNDARY LAYER DISPLACEMENT THICKNESS GROWTH.

20. ABSTRACT CONTINUED

trends but there exist significant discrepancies between them. In a general sense, the computed and measured profiles have fundamentally different shapes and their downstream development is not accurately modelled, particularly on the windside.